Optics Communications 446 (2019) 128–133

Contents lists available at ScienceDirect

Optics Communications

journal homepage: www.elsevier.com/locate/optcom

Mode-splitting based optofluidic sensing at exceptional points in tubular microcavities

Yang Wang [a], Shilong Li [b,*], Suwit Kiravittaya [c], Xiang Wu [a], Kaibo Wu [a], Xing Li [a], YongFeng Mei [a,*]

[a] Department of Materials Science, Fudan University, 220 Handan Road, Shanghai 200433, China
[b] State Key Laboratory of Infrared Physics, Shanghai Institute of Technical Physics, Chinese Academy of Sciences, 500 Yutian Road, Shanghai 200083, China
[c] Department of Electrical and Computer Engineering, Faculty of Engineering, Naresuan University, Taphoo, Muang, Phitsanulok 65000, Thailand

ARTICLE INFO

Keywords:
Exceptional points (EPs)
Whispering-gallery modes (WGMs)
Optofluidics
Refractometer

ABSTRACT

Optical microcavities have been experimentally demonstrated as an ultrasensitive device for optofluidic sensing, and monitoring of spectral shifts has been widely used in these microcavity-based optofluidic sensors. Here, spectral splitting around exceptional points (EPs) is proposed for optofluidic applications, which is based on tubular microcavities with a subwavelength-thin wall in a liquid-in-tube configuration. Both possibilities of a highly integrated optofluidic refractometer and an extinction coefficient sensor of liquid are discussed. Discussions on the sensitivity of these mode-splitting based optofluidic devices are presented to reveal their great potential in the detection of ultra-small refractive indices changes.

1. Introduction

Optofluidics, a combination of optics and microfluidics, has been widely utilized in the fields of environment, biology and chemistry [1–11]. Various optical microstructures, such as optical microcavities [1,2,12,13], plasmonic nanoantennas [14], photonic crystals [15,16] and dielectric waveguides [17] have been applied in optofluidics. Among them, the optical microcavities supporting whispering-gallery modes (WGMs), such as microtoroids [18,19], microrings [1,2,8,20] and microtubes [21–25], have attracted considerable attention for optofluidic sensing owing to their ultra-high sensitivity. However, there is an essential constraint in the optofluidic sensing with these microcavities, i.e., the frequency shift exhibits a nearly linear response to the variation in refractive indices of liquid, which sets a fundamental limitation on the ultimate performance.

In a different context, it has been recently proposed and soon after demonstrated that the sensitivity of single-nanoparticle detection based on mode splitting at exceptional points (EPs) in WGM microcavities is enhanced compared to that at diabolic points (DPs) [26]. DPs originate from the degenerated clockwise (CW) and counterclockwise (CCW) modes in the WGM microcavities with circular symmetry [27], while EPs stem from the originally degenerated CW and CCW modes with a complex-square-root topology in a circular asymmetric WGM microcavity [28–30]. Since the eigenvalues of the degenerated modes overlap at a DP, they would be separated in spectra as a single nanoparticle enters. Such phenomenon is called mode splitting and has been used for the detection of the single nanoparticle. Following a similar line of reasoning, single-nanoparticle also induces the mode splitting from EPs. However, the magnitude of the mode splitting at EPs is much greater than that at DPs for small nanoparticles, because not only the eigenvalues but also the eigenvectors of the degenerated modes collapse at the EPs [29,30]. Therefore, the sensitivity at EPs is enhanced for mode-splitting based single-nanoparticle detection, which provides a new sensing approach in theories and experiments.

Dissimilar to the single-nanoparticle detection, no mode splitting at DPs could be observed for optofluidic sensing simply because the change in liquid refractive index would not break the mode degeneracy of DPs supported by the circularly symmetric WGM microcavities. On the contrary, the refractive index change of liquid will break the mode degeneracy at EPs in the circularly asymmetric microcavities, resulting in the mode splitting. In other words, the mode splitting phenomenon at EPs could be used for the optofluidic sensing. Moreover, the resultant frequency shift near the EPs exhibits a nonlinear relation of the refractive index of liquid, and thus not constrained by the fundamental limitation mentioned above. Nevertheless, to the best of our knowledge, there have been no reports on optofluidic sensing based on the mode splitting at EPs.

In this work, we observed EPs in an optofluidic system consisting of two nano-cylinders adjoined to a microtube. A mode splitting was then generated in this optofluidic system when the liquid's refractive index changes. Both a refractometer and a liquid extinction coefficient

* Corresponding authors.
E-mail addresses: shilong.li.cn@gmail.com (S. Li), yfm@fudan.edu.cn (Y. Mei).

https://doi.org/10.1016/j.optcom.2019.04.064
Received 6 January 2019; Received in revised form 4 April 2019; Accepted 21 April 2019
Available online 25 April 2019

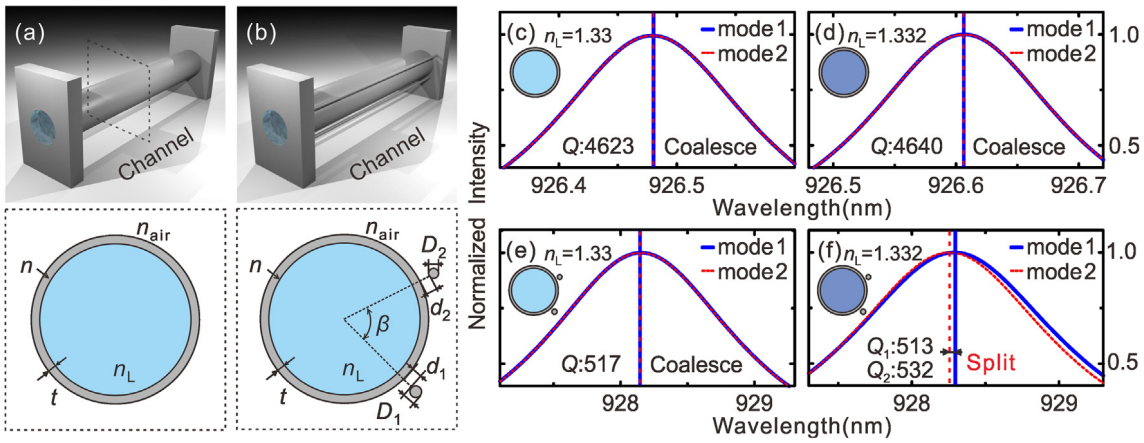

Fig. 1. A comparison between mode splitting of exceptional points (EPs) system and shifts of diabolic points (DPs) system. (a): Microtubes at diabolic points (DPs) have symmetric circular geometries with channels for liquid flow. The cross-section of microtubes exhibits ring-shaped geometry, as shown in the (a). (b): Exceptional points (EPs) are obtained by varying two nano-cylinders locations adjoined to microtubes, The cross-section of microtubes and two nano-cylinders are also presented in (b). (c)(d): The degenerate modes can be directly observed in (c) at a DP and with the small changes of refractive index of liquid in (d), the modes are still coalesced and shifts are observed. (e)(f): An EP is obtained in (e), with two modes coalesced both in resonant wavelength and Q-factor. With the same changes of refractive index, the mode splitting can be observed in (f).

sensor using the mode splitting in the vicinity of EPs are discussed. These results show the possibility of a mode-splitting based optofluidic sensing and extend the usability of the EPs microcavities.

2. Theory and methods

2.1. Model and system

Tubular microcavities, with a small mode volume and a high quality factor (Q-factor), have been used in optofluidic sensing [21–26]. Various methods, such as rolled-up nanotechnology [31], direct laser writing technique [25] and chemical-template synthesis [31,32], have been proposed to fabricate such tubular microstructures. The microtubes used in an optofluidic system basically have a symmetric geometry, as shown in Fig. 1(a) [1,21]. The cross-section of the microtubes is also represented. With an assumption that there is a continuous translational symmetry along the axial direction [28], the microtube can be simplified as a microring in the two-dimensional cross-sectional plane.

In the optofluidic sensing using microtubes, there are three different configurations: the liquid-in-tube, where liquid is only in the inner core; the hollow-tube-in-liquid, where liquid is only in the outside; and the tube-in-liquid with both parts filling with the liquid [33]. Here, we use the liquid-in-tube configuration in optofluidics, with the liquid refractive index $n_L = 1.33$ (Extinction coefficient of liquid $k_L = 0$, assuming no gain and loss). Other parameters in Fig. 1(a) are as following: the inner diameter $D_i = 2.88$ μm, the thickness of tube $t = 160$ nm, the refractive indices of microtubes $n = 2.0$ and the air $n_{air} = 1$, which are kept constants unless otherwise noted.

Following the single-nanoparticle detection system [27,29,30,34], a configuration to find EPs in optofluidics is presented in Fig. 1(b). We design two ultra-thin cylinders adjoined to the microtubes, where the configuration can be also simplified into ring-shaped geometry with two nano-particles, owing to the same assumption in Fig. 1(a). The cross-section in Fig. 1(b) indicates that two cylinders are defined by the distance d_i from microtubes, the diameter D_1 and D_2 of each cylinder and the angle β between two cylinders. In this work, $d_1 = 16$ nm and $D_1 = 137.6$ nm are defined for the first cylinder, while only $d_2 = 24$ nm is defined for the second, leaving the size of second particle D_2 and angle β as variational parameters to be close to EPs. In addition, other parameters are set to be the same as those in symmetric tubes in Fig. 1(a). These models might be realized in the experiments by direct laser writing [25] and photoluminescence (PL) microscopy measurement [21] for optofluidics.

2.2. Finite element methods

To approach the EPs and subsequent results, Maxwell equations are utilized and simplified to a three-dimensional scalar Helmholtz equation (1) in the cylindrical coordinate system, with the assumption of infinite length in axial direction [28,35],

$$\nabla^2\psi + n^2(\rho,\phi,z)\,\psi\frac{\omega^2}{c^2} = 0, \tag{1}$$

where ψ is the wave function, ω is the complex frequency, c is the speed of light in the vacuum, and $n(\rho,\phi,z)$ is the piecewise constant refractive index [21]. The finite-element methods (FEM) are adopted to solve the two-dimensional differential equation reduced from Maxwell's equations with Sommerfeld radiation wave conditions at infinity, which express the equations associated boundary conditions as a set of linear equations that can be solved computationally using linear algebra [36]. In addition, we mainly consider transverse magnetic (TM) polarization mode in this work.

3. Results and discussion

3.1. Mode splitting for optofluidic sensing

Our results show that the EPs are observed with appropriate parameter values in optofluidic system and mode splitting can be generated when the refractive indices change. The comparison between microcavities at a DP and an EP are illustrated in Fig. 1(c)–(f), respectively. Fig. 1(c) and (d) show the microcavities at a DP with n_L changing from 1.330 to 1.332. Blue solid line and red dashed line represent two degeneracy modes in the same circular conditions. The peak locations are highlighted by the vertical blue solid lines and red dashed lines, and the Q-factors are calculated according to the formula: $Q = \lambda/\Delta\lambda$, where λ is the resonance wavelength and $\Delta\lambda$ is the full width at half maximum (FWHM) [19]. The resonance peak locations and Q-factors in Fig. 1(c) and (d) indicate that two modes are absolutely coalesced regardless of n_L value. Upon the changes of refractive indices, only resonant wavelength shifts can be observed in the spectra. The reason is that the whole system is consistently symmetric with the changes of refractive indices, leading to constant degenerated modes.

On the contrary, distinct results are found at an EP. Fig. 1(e) and (f) show the EP and the mode splitting for optofluidic sensing. In Fig. 1(e) two modes can be coalesced when $D_2 = 141.760$ nm and $\beta = 1.075\,061$. The lower Q-factor and the slight shift in the resonance wavelength can be attributed to the extra scattering coupling to two cylinders compared

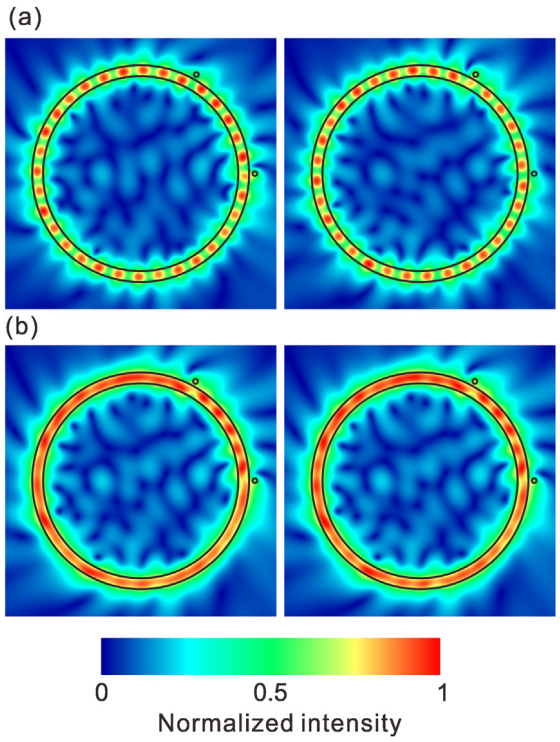

Fig. 2. Electric field intensity of resonant modes by varying D_2 and β parameters in tubular microcavities with the subwavelength thin walls. (a): Two coupling modes are far away from the EP, and the stationary wave can be directly observed in the geometry. Meanwhile, the modes are different in the electric intensity distribution. Importantly, strong electric intensity is found at the outside of tubular surface, making the interaction between tubular geometry and particles more sensitive than disk geometry. (b): The coupling modes are ultra-close to the EP, with same travel wave can be found in the figure. Similarly, strong electric intensity distribution is found at outside of the tubular surface.

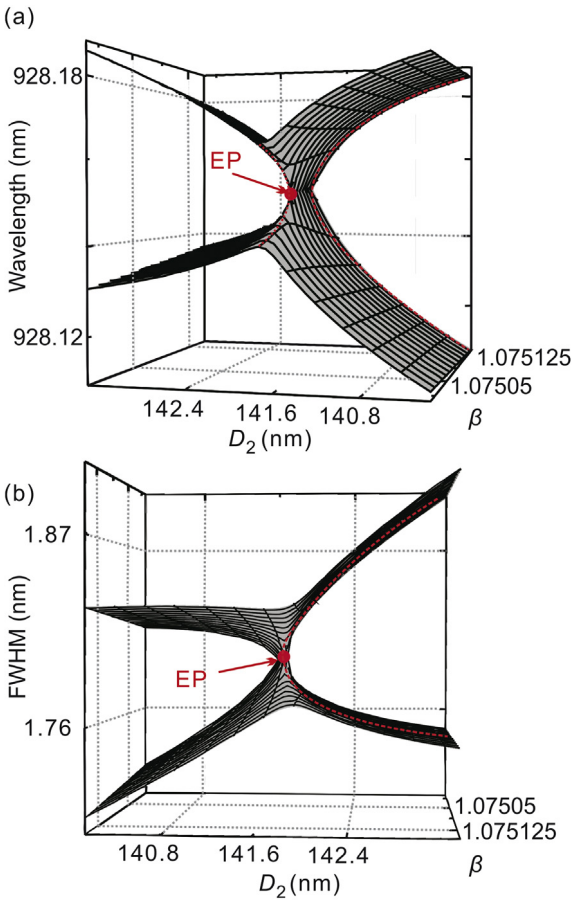

Fig. 3. Topological structures of the EP in the β - D_2 parameter space. (a): Resonance wavelength of two coupling modes in the parameter space. (b): The full width at half maximum (FWHM) of two coupling modes in the parameter space. The red points represent the EP and red dashed lines illustrate the distinguished square-root relationship as nonlinear behaviors . (For interpretation of the references to color in this figure legend, the reader is referred to the web version of this article.)

with the circular symmetric microcavities. More importantly, the mode splitting in the microcavities is fulfilled under small change of the refraction index, such as $n_L = 1.332$, as illustrated in Fig. 1(f). Not only at resonance wavelength position but also at Q-factors can the mode splitting be observed. The mechanism behind such splitting could be explained as following: the change of refraction index can be regarded as a small perturbation to the original system where two modes is ultra-close to the EP, and the perturbation causes two modes to shift away from the singularities, resulting in the splitting.

3.2. Mode splitting in subwavelength-thin walled tubular microcavities

Compared with the mode splitting studied in microdisks [27,29,30,34], the mode splitting here is particularly based on tubular geometry and the subwavelength-thin wall. Such unique features of tubular microcavities have been investigated, suggesting that weak light confinement faculties of the geometry result in high sensitivity for detection, especially in optofluidics [21]. Thus, we systematically probe the electric field intensity and topological structures around the EP to explore the sensing potential with such structures. Fig. 2 indicates the electric fields of resonant modes when the parameters are around the EP. Fig. 2(a) shows two splitting mode pairs away from the EP, where the parameters are set as $D_2 = 140.800$ nm and $\beta = 1.075\,000$. The stationary wave modes can be directly found due to the coupling of CW and CCW modes, and the discrepancy with the conventional disks is illustrated by the higher distribution of electric field intensity near the outside surface of tubular structures. As a comparison, when the parameters are close to the EP with $D_2 = 141.760$ nm and $\beta = 1.075\,061$, as expected, two modes would become similar in the electric field intensity, demonstrating that the systems are close to the EP, as presented in Fig. 2(b). The intensity of electric fields in the near-field also illustrates the stronger evanescent fields in the structures. The mechanism of the stronger evanescent fields can be explained as the reflection happening at the inner surface where there is an interaction between microcavities and liquid. What is more, the subwavelength-thin wall contributes to the much stronger coupling of evanescent fields to environment and small perturbation than thick wall due to the reduction of light confinement. In other words, despite the lower Q-factors, the tubular microcavities make it more sensitive to perturbation of the near-field, for example, the particles and the refractive index, owing to the enhanced intrinsic backscattering and smaller wall size than resonance wavelength.

Meanwhile, we discuss the topological structures of two coupling pairs around the EP, as shown in Fig. 3. Fig. 3(a) and (b) show the resonant wavelength and the FWHM in the β-D_2 parameter space, respectively. The EP are as critical points in the topology structures highlighted in red. Moreover, resonant wavelength and FWHM clearly demonstrate the complex-square-root topology around EPs, as marked by red dashed lines. These results illustrate that nonlinear behaviors of the mode splitting can be applied in optofluidic sensing.

3.3. Refractometer

Attributed to nonlinear behaviors around the EP shown in Fig. 3, the mode splitting reveals its applicability in optofluidic sensing. Most

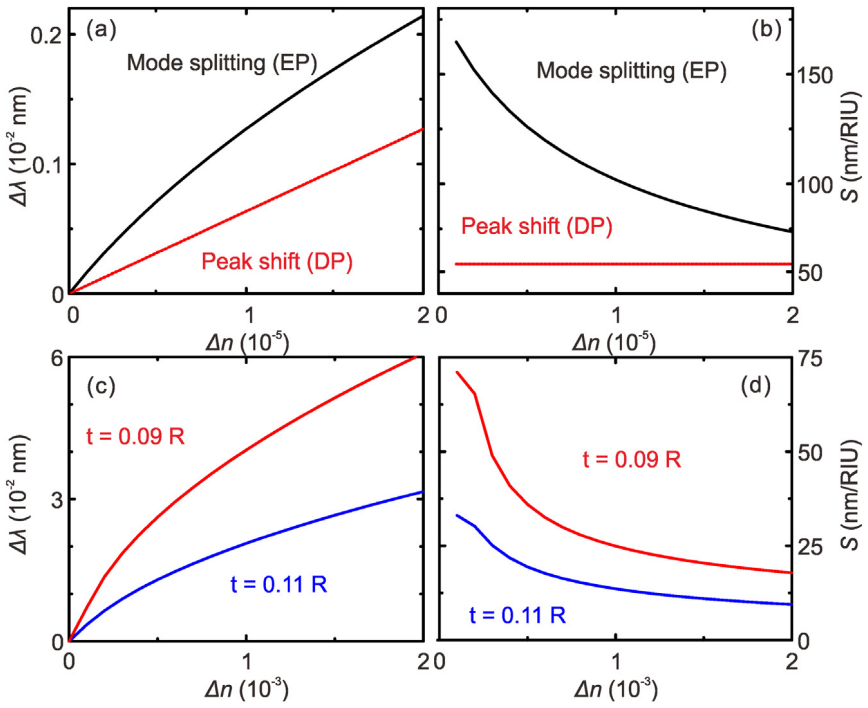

Fig. 4. The mode splitting can be used as refractometer and modulation of refractometer. (a): The mode splitting is represented as splitting of two coupling modes in the EP system (dark solid line), in contrast to the peak shifts of resonant wavelength in the DP system (red dashed line). With ultra-small changes of refractive indices (~10^{-5}), the mode splitting is larger than the peak shift. (b): The sensitivities of mode splitting imply that with smaller changes of refractive indices, larger sensitivities will be achieved. (c): The mode splitting is modulated by the wall thickness of tubular microcavities. (d): The sensitivities of mode splitting indicate that larger sensitivities are obtained with thinner wall thickness . (For interpretation of the references to color in this figure legend, the reader is referred to the web version of this article.)

extensively, the refractometer utilized to detect refractive indices of liquid has been widely investigated by many different methods, such as optical microcavities [37–40] and optical fibers [41–44]. For optical microcavities, most of the works deduce the refractive index from the shifts of resonant wavelength based on WGMs. However, the key problems of these techniques are the limitation of detection (LOD) and maximum sensitivities. More importantly, the LOD and sensitivities are naturally constrained because of the inherent linear relation with frequency shifts and refractive index of liquid, inducing the puzzle for detection of ultra-small changes of refractive index. As an extraordinary method, novel nonlinear behaviors of EP systems can be utilized as highly sensitive refractometer. Since two degeneracy modes will split both in resonant wavelength and FWHM, we mainly focus on the resonant wavelength splitting as a congruous contrast with the wavelength shifts at DPs.

Fig. 4(a) shows the mode splitting of resonant wavelength at an EP and wavelength shifts at a DP of two degeneracy mode with the increasing refractive index of liquid. The initial refractive index of liquid is 1.330 and the extinction coefficient of liquid is assumed as 0. The black solid line shows the wavelength splitting at the EP according to $\lambda_r = \Delta\lambda_{\Delta n} - \Delta\lambda_0$, where $\Delta\lambda_{\Delta n}$ is the wavelength difference of two splitting modes, the change of refractive index $\Delta n = n_L - 1.330$ and $\Delta\lambda_0$ is the wavelength distance of two splitting modes when $n_L = 1.330$. The red dashed line shows the wavelength shifts at the DP, defined with $\lambda_r = \lambda_{\Delta n} - \lambda_0$, where $\lambda_{\Delta n}$ is the degenerate resonant wavelength while λ_0 is the degenerate resonant wavelength when $n_L = 1.330$. Though near-linear relation around the DP is based on the frequency shifts, the wavelength, defined as $1/\lambda = nf/c$, can also be approximately regarded as the near-linear relation due to the ultra-small ranges of refractive index changes, as shown in Fig. 4(a). As the refractometer, the splitting exhibits larger values than the shifts, with Δn ranging from 0 to 2×10^{-5}. Moreover, the results demonstrate that the mode splitting demonstrates a square-root relation $(\Delta n)^{1/2}$ corresponding to the two-order EP systems [26] in contrast to the near-linear relations of DP, as presented in Fig. 4(a). Therefore, when the changes of refractive index are ultra-small (far smaller than one refractive index unit (RIU)), the splitting would be ultra-larger than the shifts in the DPs.

Furthermore, as the most significant properties for sensing, the sensitivities using shifts in the DP and the splitting in the EP are shown in Fig. 4(b), with Δn ranging from 1×10^{-6} to 2×10^{-5}. Calculated according to $S = d\lambda_r/d(\Delta n)$, the sensitivities at the EP and DP are in the black solid line and the red dashed line, respectively. The stable sensitivities at the DP in small ranges could clearly be observed, making it hard to differentiate ultra-low concentration change in liquid owing to detector limitation. Moreover, distinct singularities result in the high sensitivity around the EP, as the nontrivial topological structures show. In Fig. 4(b), the sensitivity can reach at 165 nm RIU^{-1} with $\Delta n = 1 \times 10^{-6}$, threefold larger than the sensitivity at the DP (63 nm RIU^{-1}) under the same Δn, demonstrating that the sensitivity at EPs can be higher than at DPs with the same size of microcavities. Especially when there are extremely small liquid refractive index changes from the EP, like $\Delta n < 1 \times 10^{-6}$, the sensitivities would also be higher, which might theoretically have large LOD in the EPs system. Furthermore, however, if the EPs system is applied in the experiments, the noise from temperature fluctuation [45] and variation of structure as well as detectivity limitation of measurement might influence the LOD of system. In that case, calibration method and criteria like using PL microscopy and multiple measurement might reduce the influence of noise.

Although the relatively high sensitivities in EPs break the limitation, the modulation of sensitivities remains obscure in the system. As higher sensitivities would be possible under the condition of subwavelength thin wall, the thickness of wall needs to be considered to realize the optimization of sensitivities. Despite the change in thickness, the outermost radius (R) of microtubes is invariable. The results demonstrating the relation between thickness and splitting with the refractive index ranging from 1.330 to 1.3302 are presented in Fig. 4(c). The red and blue lines represent the thickness $t = 0.09R$ and $t = 0.11R$, respectively. For parameters, the EPs are ultra-closed when $D_2 = 133.504$ nm and $\beta = 1.072\ 617$ ($t = 0.09R$) or $D_2 = 140.416$ nm and $\beta = 1.074\ 957$

($t = 0.11R$). Obviously, larger splitting is observed when $t = 0.09R$ compared with $t = 0.11R$, with the mode splitting of both thicknesses conform to the square-root relation. These results illustrate that the stronger intrinsic backscattering can lead to higher sensitivities due to the thinner wall thickness. The sensitivities are also shown in Fig. 4(d), using the same formula in Fig. 4(b) with Δn ranging from 1×10^{-4} to 2×10^{-3}. As expected, the results show the higher sensitivities in $t = 0.09R$ compared to $t = 0.11R$. These results including the nonlinear behavior and sensitivities modulation clearly justify the potential of the system to be applied as refractometer in optofluidic sensing.

3.4. Extinction coefficient sensing of liquid gain mediums

Extinction coefficient, as considered, is a vital field in environmental, chemical and biological concentration sensing [46]. Basically, the extinction coefficient k is also the imaginary part of the complex refractive indices of liquid $n = n_L + ik$, representing the gain or loss of the medium. Importantly, the liquid gain mediums, such as fluorescent dyes and biological aqueous buffers, have been widely utilized in lasers and sensors [2,47–53]. Such as fluorescent dyes, k is depended on the dye concentration, which directly impacts upon the optical properties such as lasing threshold [47]. Moreover, the concentration-depended extinction coefficient k would change with the photochemical degradation of fluorescent dye-doped polymers under lasing conditions [48]. However, it is hard to precisely detect the ultra-small changes of k by deducing from the intensity with constant refractive indices n using liquid gain mediums. Even for the normal microcavities, the peak locations of resonance remain unchanged when only the extinction coefficient of liquid changes. More importantly, since in our work the mode splitting with non-linear behaviors around EPs is ultra-sensitive with the changes of liquid, it is possible to detect ultra-small changes of extinction coefficient of liquid.

To simplify the problem, we define the refractive index of liquid as a constant value ($n_L = 1.330$) in this section. For extinction coefficient, $k > 0$ means the absorption of liquid and $k < 0$ means the gain. Here, we mainly discuss about $k < 0$, due to the gain medium properties. The results are shown in Fig. 5. Fig. 5(a) shows the mode splitting distance at an EP (black solid line) with Δk changes. The mode splitting is defined as $\lambda_a = \Delta\lambda_k - \Delta\lambda_0$, where $\Delta\lambda_k$ is the wavelength distance of two splitting modes, and $\Delta\lambda_0$ is the wavelength distance of two splitting modes when $k = 0$. Moreover, the wavelength shifts at a DP (red dashed line) are also shown in Fig. 5(a), according to $\lambda_a = \lambda_k - \lambda_0$. As expected, the splitting rapidly increases with small changes from the EP, while the resonant wavelength locations at the DP are nearly zero with tiny fluctuation ranging from 0 to -3×10^{-4}. Furthermore, the splitting follows the two-order EP system, exhibiting a complex-square-root relationship between splitting and changes. The sensitivities for mode splitting and wavelength shift have been calculated in Fig. 5(b), stipulated by $S_a = d\lambda_a/d(\Delta k)$. With smaller changes from the EP, the sensitivity can be higher, such as the sensitivity can reach 155.2 nm k^{-1} at gain changes $k = -0.000\,01$ from $k = 0$. Compared to the sensitivity for the DP which is approximated to zero, the EP system can be a new method and technology for detecting the extinction coefficient for those who have similar refractive indices and tiny extinction coefficient difference in liquid circumstance. What is more, the absorption sensing as $k > 0$ could also have higher sensitivities in EPs system compared with DPs system, as shown in Fig. S1 of Supplementary material, which illustrates the broad application potential of EPs system for extinction coefficient test.

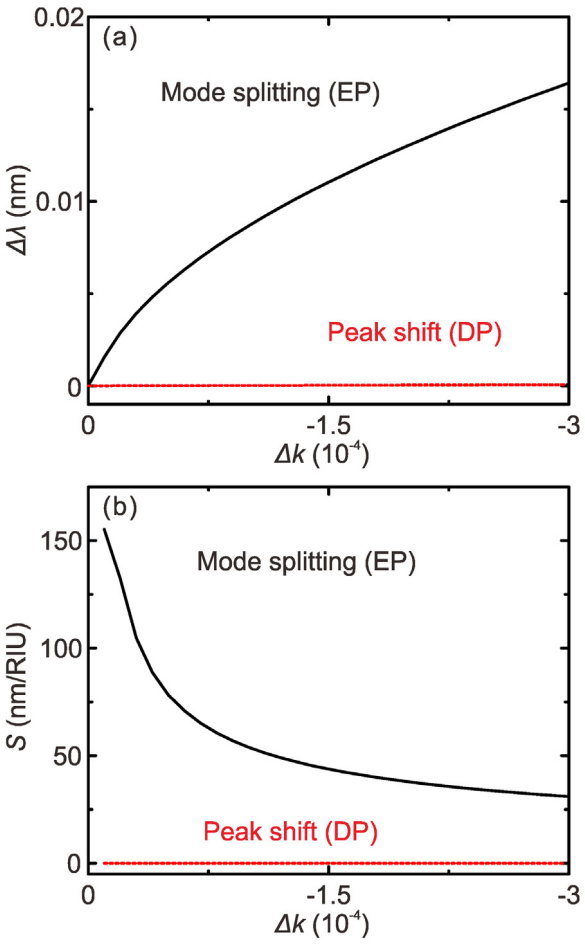

Fig. 5. Mode splitting can be used as liquid extinction coefficient sensing. (a) The mode splitting in the EP system is in contrast to the peak shifts in the DP system along with the changes of extinction coefficient, the mode splitting increases rapidly and the peak shift is stably ultra-close to 0. (b). The sensitivity of mode splitting indicates the superiority of EP system.

4. Conclusion

In optofluidic systems using tubular microcavities, we have observed EPs and the associated mode splitting. A nonlinear response of the mode splitting around the EPs has been observed, which provides a high sensitivity for an ultra-small change in refractive indices, and thus could be applied as refractometers. Moreover, the extinction coefficient of liquid could be detected by the mode splitting mechanism, though it is hard in the traditional optical microcavities using DPs. This EPs optofluidic system thus breaks the fundamental limitation of the symmetric counterpart and renders itself a promising candidate for small molecule detection and ultra-low concentration detection in an on-chip manner.

Acknowledgments

This work is supported by the Natural Science Foundation of China (Nos. 51322201 and U1632115), the Science and Technology Commission of Shanghai Municipality, China (No. 17JC1401700) and the Changjiang Young Scholars Program of China. One of the authors (SK) acknowledges financial support from the Research Chair Grant, the National Science and Technology Development Agency (NSTDA), Thailand. SK also thanks the Fudan Fellow Program, People's Republic of China. The author (SL) acknowledges the financial support of the International Postdoctoral Exchange Fellowship Program, China (No. 20170010).

Appendix A. Supplementary data

Supplementary material related to this article can be found online at https://doi.org/10.1016/j.optcom.2019.04.064.

References

[1] D. Psaltis, S.R. Quake, C.H. Yang, Developing optofluidic technology through the fusion of microfluidics and optics, Nature 442 (2006) 381–386.
[2] X.D. Fan, I.M. White, Optofluidic microsystems for chemical and biological analysis, Nature Photon. 5 (2011) 591–597.
[3] W. Lee, Q.S. Chen, X.D. Fan, D.K. Yoon, Digital DNA detection based on compact optofluidic laser with ultra-low sample consumption, Lab. Chip 16 (2016) 4770.
[4] C. Monat, P. Domachuk, B.J. Eggleton, Integrated optofluidics: A new river of light, Nature Photon. 1 (2007) 106–114.
[5] F. Vollmer, S. Arnold, Whispering-gallery-mode biosensing: label-free detection down to single molecules, Nat. Methods 5 (2008) 591–596.
[6] C. Szydzik, A.F. Gavela, S. Herranz, J. Roccisano, M. Knoerzer, P. Thurgood, K. Khoshmanesh, A. Mitchell, L.M. Lechuga, An automated optofluidic biosensor platform combining interferometric sensors and injection moulded microfluidics, Lab. Chip 17 (2017) 2793–2804.
[7] X.D. Fan, I.M. White, S.I. Shopova, H.Y. Zhu, J.D. Suter, Y.Z. Sun, Sensitive optical biosensors for unlabeled targets: a review, Anal. Chim. Acta 620 (2008) 8–26.
[8] H.L. Liu, Y. Shi, L. Liang, L. Li, S.S. Guo, L. Yin, Y. Yang, A liquid thermal gradient refractive index lens and using it to trap single living cell in flowing environments, Lab. Chip 17 (2017) 1280–1286.
[9] I.M. White, H. Oveys, X.D. Fan, T.L. Smith, J.Y. Zhang, Integrated multiplexed biosensors based on liquid core optical ring resonators and antiresonant reflecting optical waveguides, Appl. Phys. Lett. 89 (2006) 191106.
[10] I.M. White, H. Oveys, X.D. Fan, Liquid-core optical ring-resonator sensors, Opt. Lett. 31 (2006) 1319.
[11] M. Kim, M. Pan, Y. Gai, S. Pang, C. Han, C.H. Yang, S.K.Y. Tang, Optofluidic ultrahigh-throughput detection of fluorescent drops, Lab. Chip 15 (2015) 1417–1423.
[12] H.Y. Zhu, I.M. White, J.D. Suter, P.S. Dale, X.D. Fan, Analysis of biomolecule detection with optofluidic ring resonator sensors, Opt. Express 15 (2007) 9139.
[13] W.Z. Song, A.Q. Liu, S. Swaminathan, C.S. Lim, P.H. Yap, T.C. Ayi, Determination of single living cell's dry/water mass using optofluidic chip, Appl. Phys. Lett. 91 (2007) 223902.
[14] K.A. Willets, R.P.V. Duyne, Localized surface plasmon resonance spectroscopy and sensing, Annu. Rev. Phys. Chem. 58 (2007) 267–297.
[15] M.R. Lee, P.M. Fauchet, Two-dimensional silicon photonic crys- tal based biosensing platform for protein detection, Opt. Express 15 (2007) 4530–4535.
[16] Y.N. Zhang, Y. Zhao, T.M. Zhou, Q.L. Wu, Applications and developments of on-chip biochemical sensors based on optofluidic photonic crystal cavities, Lab. Chip 18 (2018) 57–74.
[17] N. Skivesen, R. Horvath, H.C. Pedersen, Peak-type and dip-type metal-clad waveguide sensing, Opt. Lett. 30 (2005) 1659–1661.
[18] K.J. Vahala, Optical microcavities, Nature 424 (2003) 839–846.
[19] A.M. Armani, R.P. Kulkarni, S.E. Fraser, R.C. Flagan, K.J. Vahala, Label-free, single-molecule detection with optical microcavities, Science 317 (2007) 783–787.
[20] K. Scholten, X.D. Fan, E.T. Zellers, A microfabricated optofluidic ring resonator for sensitive, high-speed detection of volatile organic compounds, Lab. Chip 14 (2014) 3873–3880.
[21] G.S. Huang, V.A. Bolaños Quiñones, F. Ding, S. Kiravittaya, Y.F. Mei, O.G. Schmidt, Rolled-up optical microcavities with subwavelength wall thicknesses for enhanced liquid sensing applications, ACS Nano 4 (2010) 3123–3130.
[22] J. Zhang, J. Zhong, Y.F. Fang, J. Wang, G.S. Huang, X.G. Cui, Y.F. Mei, Roll up polymer/oxide/polymer nanomembranes as a hybrid optical microcavity for humidity sensing, Nanoscale 6 (2014) 13646–13650.
[23] V.A. Bolaños Quiñones, L.B. Ma, S.L. Li, M. Jorgensen, S. Kiravittaya, O.G. Schmidt, Localized optical resonances in low refractive index rolled-up microtube cavity for liquid-core optofluidic detection, Appl. Phys. Lett. 101 (2012) 151107.
[24] A. Madani, S.M. Harazim, V.A. Bolaños Quiñones, M. Kleinert, A. Finn, E.S. Ghareh Naz, L.B. Ma, O.G. Schmidt, Optical microtube cavities monolithically integrated on photonic chips for optofluidic sensing, Opt. Lett. 42 (2017) 486–489.
[25] Y.L. Li, Y.F. Fang, J. Wang, L. Wang, S.W. Tang, C.P. Jiang, L.R. Zheng, Y.F. Mei, Integrative optofluidic microcavity with tubular channels and coupled waveguides via two-photon polymerization, Lab. Chip 16 (2016) 4406–4414.
[26] Y.Z. Qin, Y.F. Fang, L. Wang, S.W. Tang, S.L. Shu, Z.W. Liu, Y.F. Mei, Surface wave resonance and chirality in a tubular cavity with metasurface design, Opt. Commun. 417 (2018) 42–45.
[27] W.J. Chen, Ş. K. Özdemir, G.M. Zhao, J. Wiersig, L. Yang, Exceptional points enhance sensing in an optical microcavity, Nature 548 (2017) 192–196.
[28] Y.F. Fang, S.L. Li, S. Kiravittaya, Y.F. Mei, Exceptional points in rolled-up tubular microcavities, J. Opt. 19 (2017) 095101.
[29] J. Wiersig, Structure of whispering-gallery modes in optical microdisks perturbed by nanoparticles, Phys. Rev. A 84 (2011) 063828.
[30] J. Wiersig, Enhancing the sensitivity of frequency and energy splitting detection by using exceptional points: Application to microcavity sensors for single-particle detection, Phys. Rev. Lett. 112 (2014) 203901.
[31] Y.F. Mei, G.S. Huang, A.A. Solovev, E.B. Ureña, I. Monch, F. Ding, T. Reindl, R.K.Y. Fu, P.K. Chu, O.G. Schmidt, Versatile approach for integrative and functionalized tubes by strain engineering of nanomembranes on polymers, Adv. Mater. 20 (2008) 4085–4090.
[32] Y.P. Rakovich, S. Balakrishnan, J.F. Donegan, T.S. Perova, R.A. Moore, Y.K. Gun'ko, The. Fabrication, Fluorescence. Dynamics, The fabrication fluorescence dynamics and whispering gallery modes of aluminosilicate microtube resonators, Adv. Funct. Mater. 17 (2007) 1106–1114.
[33] F.Y. Zhao, T.R. Zhan, G.S. Huang, Y.F. Mei, X.H. Hu, Liquid sensing capability of rolled-up tubular optical microcavities: a theoretical study, Lab. Chip 12 (2012) 3798–3802.
[34] J. Wiersig, Sensors operating at exceptional points: General theory, Phys. Rev. A 93 (2016) 033809.
[35] Y.F. Fang, S.L. Li, Y.F. Mei, Modulation of high quality factors in rolled-up microcavities, Phys. Rev. A 94 (2016) 033804.
[36] J. Wang, T.R. Zhan, G.S. Huang, P.K. Chu, Y.F. Mei, Optical microcavities with tubular geometry: properties and applications, Laser Photonics Rev. 8 (4) (2014) 521–547.
[37] A.M. Armani, K.J. Vahala, Heavy water detection using ultra-high-q microcavities, Opt. Lett. 31 (2006) 1896–1898.
[38] E. Chow, A. Grot, L.W. Mirkarimi, M. Sigalas, G. Girolami, Ultracompact biochemical sensor built with two-dimensional photonic crystal microcavity, Opt. Lett. 29 (2004) 1093–1095.
[39] A. Ksendzov, Y. Lin, Integrated optics ring-resonator sensors for protein detection, Opt. Lett. 30 (2005) 3344–3346.
[40] S.W. Tang, Y.F. Fang, Z.W. Liu, L. Zhou, Y.F. Mei, Tubular optical microcavities of indefinite medium for sensitive liquid refractometers, Lab. Chip 16 (1) (2016) 182.
[41] L. Rindorf, O. Bang, Highly sensitive refractometer with a photonic-crystal-fiber long-period grating, Opt. Lett. 33 (2008) 563–565.
[42] C.F. Chan, C.K. Chen, A. Jafari, A. Laronche, D.J. Thomson, J. Albert, Optical fiber refractometer using narrowband cladding-mode resonance shifts, Appl. Opt. 7 (2007) 1142–1149.
[43] N. Zhang, K.W. Li, Y. Cui, Z.F. Wu, P.P. Shum, J.L. Auguste, X.Q. Dinh, G. Humbert, L. Wei, Ultra-sensitive chemical and biological analysis via specialty fibers with built-in microstructured optofluidic channels, Lab. Chip 18 (2018) 655–661.
[44] C. Caucheteur, P. Megret, Demodulation technique for weakly tilted fiber bragg grating refractometer, IEEE Photon. Technol. Lett. 17 (2005) 2703–2705.
[45] E. Kim, M.D. Baaske, F. Vollmer, Towards next-generation label-free biosensors: recent advances in whispering gallery mode sensors, Lab. Chip 17 (2017) 1190.
[46] C. Vallance, A.A.P. Trichet, D. James, P.R. Dolan, J.M. Smith, Open-access microcavities for chemical sensing, Nanotechnology 27 (2016) 274003.
[47] M.C. Gather, S.H. Yun, Single-cell biological lasers, Nature Photon. 5 (2011) 406–410.
[48] T. Reynolds, N. Riesen, A. Meldrum, X.D. Fan, J.M.M. Hall, T.M. Monro, A. François, Fluorescent and lasing whispering gallery mode microresonators for sensing applications, Laser Photonics Rev. 11 (2017) 1600265.
[49] V. Marx, Probes: paths to photostability, Nat. Methods 12 (2015) 187–190.
[50] X. Yang, W.X. Shu, Y.Q. Wang, Y. Gong, C.Y. Gong, Q.S. Chen, X.T. Tan, G.D. Peng, X.D. Fan, Y.J. Rao, Turbidimetric inhibition immunoassay revisited to enhance its sensitivity via an optofluidic laser, Biosens. Bioelectron. 131 (2019) 60–66.
[51] C.Y. Gong, Y. Gong, X. Zhao, Y. Luo, Q. Chen, X. Tan, Y. Wu, X. Fan, G. Peng, Distributed fibre optofluidic laser for chip-scale arrayed biochemical sensing, Y. J. Rao Lab. Chip 18 (2018) 2741–2748.
[52] C.Y. Gong, Y. Gong, M. Oo, Y. Wu, Y.J. Rao, X.T. Tan, X.D. Fan, Sensitive sulfide ion detection by optofluidic catalytic laser using horseradish peroxidase (HRP) enzyme, Biosens. Bioelectron. 96 (2017) 351–357.
[53] C.Y. Gong, Y. Gong, Q.S. Chen, Y.J. Rao, G.D. Peng, X.D. Fan, Reproducible fiber optofluidic laser for disposable and array applications, Lab. Chip 17 (20) (2017) 3431–3436.